

# Modeling aperiodic magnetospheric oscillations

Murchana Khusroo and Madhurjya P. Bora\*

Physics Department, Gauhati University, Guwahati 781014, India



(Received 9 April 2018; revised manuscript received 20 September 2018; published 17 January 2019)

We present an analysis of a Hall-magnetohydrodynamics model of the magnetospheric plasma with finite Larmor radius effect. Through a bifurcation analysis of the resultant nonlinear system, we show that this nonlinear model does not possess a limit cycle, which rules out regular periodic oscillations with constant amplitude. However, it does result in a train of magnetosonic solitons, localized in space, with amplitudes increasing in time, which are largely in agreement with what is usually observed in the magnetopause region. We call these oscillations *aperiodic magnetospheric oscillations*. We emphasize that most of the train of solitary oscillations observed by the *Cluster* fleet and other spacecrafts do not have constant amplitudes: they either continuously increase or decrease. These train of solitons with nonconstant amplitudes is a primary solution of our model.

DOI: [10.1103/PhysRevE.99.013205](https://doi.org/10.1103/PhysRevE.99.013205)

## I. INTRODUCTION

Solitary waves, most commonly known as solitons, are nonlinear oscillatory structures which are routinely observed in near-earth plasmas and in the boundary layers of the earth's magnetosphere [1,2]. Since its demonstration by Scott Russel in 1844, solitons have now become one of the most widely studied phenomena in fluids including plasmas. Though solitons can be found in a controlled laboratory as well as in various natural situations, space plasma is such an environment, where observations of solitary oscillations have become easier due to advances in space exploration. The space-borne experiments have now provided us with valuable information about different regions of the magnetosphere and their physics. Many magnetosonic solitons are reported to be observed by *Cluster* spacecrafts near the bowshock-magnetopause crossing, magnetosheath, and cusp region of the magnetosphere. One of the first series of observations of magnetosonic solitons was by the *Cluster* spacecraft in 2002 [3–5].

Regarding the magnetic oscillations in the magnetopause and magnetosheath regions, we have only limited knowledge about them, and the origin and behavior of these oscillations are not yet fully understood. These oscillations seem to be nonlinear and quasistatic in nature and are usually present with ion temperature anisotropy with  $T_{i\perp} > T_{i\parallel}$  with an anticorrelation with density fluctuation [6–8]. The size of these oscillatory structures are within a few ion Larmor radii. In most of the cases, these oscillations have nonconstant amplitudes and are seen as a train of solitons (localized in space) with either continuously increasing or decreasing amplitudes. The usual interpretation of these structures is considered as nonlinear saturation of the mirror instability, which satisfies the mirror instability condition [9]

$$\frac{T_{i\perp}}{T_{i\parallel}} > 1 + \frac{1}{\beta_{\perp}}, \quad (1)$$

where  $\beta_{\perp}$  is the perpendicular plasma  $\beta$ . As we can see that the mirror instability requires a temperature anisotropy with a sufficiently large  $\beta$ . It is a zero-frequency instability which is driven by wave-particle resonance. Apparently, similar oscillations are also observed in other planetary magnetospheres [10] and cometary environments [11]. However, it has been shown that these train of magnetic pulses can also be interpreted as slow-mode magnetosonic solitons resulting out of a Hall-magnetohydrodynamics (MHD) plasma model [12]. Other authors have tried to explain these oscillations as a solution of MHD plasma equations, with mirror mode instability as the trigger mechanism [13]. Theoretical studies have revealed that many underlying physical phenomena can govern the formation of these structures. One such phenomenon is the finite Larmor radius (FLR) effect, which can play an important role in the formation of structures in the current layer of the magnetotail and magnetopause region as well as the cusp region. Apparently the effects which take place within the scale length of ion Larmor radii are called FLR effects. Primarily, the FLR effect enters the ideal MHD equations through the electron pressure term in the generalized Ohm's law, which becomes important when spatial scale length  $L$  becomes comparable to the ion Larmor radius  $r_L$  [14]:

$$\frac{\nabla p_e / (ne)}{\mathbf{v} \times \mathbf{B}} \sim \frac{T_i}{evBL} \sim \frac{m_i v_{thi}}{eBL} \sim \frac{r_L}{L} \gtrsim 1. \quad (2)$$

Physically,  $L$  represents the plasma or field line inhomogeneities [1]. Plasma expansion across different plasma layers leads to formation of filamentary structures where FLR effects become important. In the magnetopause layer, specular reflection of solar wind plasma causes formation of a boundary layer which is about  $\sim 10r_L$  thick [15], where the FLR effects are supposed to be responsible for formation of microstructures [15,16].

In this work, we analyze the Hall-MHD model of these oscillations with the FLR effect, which leads to a nonlinear dynamical model that can produce such a train of solitons with nonconstant amplitudes. In Sec. II we put forward our plasma

\*mpbora@gauhati.ac.in



model, where we have incorporated the FLR term through the generalized Ohm's law. In Sec. III we outline a general approach where the equations are reduced to two differential equations that describes the flow of plasma. In Sec. IV we present a nonlinear dynamical analysis of the problem with and without the FLR effect. In Sec. V we compare our findings with observational data from the *Cluster* spacecrafts. Finally in Sec. VI we summarize and conclude our work.

## II. THE PLASMA MODEL

We consider the basic Hall-MHD equations with finite Larmor radius term [17]

$$\frac{\partial \rho}{\partial t} + \nabla \cdot (\rho \mathbf{v}) = 0, \quad (3)$$

$$\rho \frac{d\mathbf{v}}{dt} = \mathbf{J} \times \mathbf{B} - \nabla \cdot \mathbb{P}, \quad (4)$$

$$\begin{aligned} \mathbf{E} + \mathbf{v} \times \mathbf{B} &= \frac{1}{e\rho} (m_i - m_e)(\mathbf{J} \times \mathbf{B}) - \frac{1}{eN} \nabla p_e \\ &\approx \frac{1}{eN} (\mathbf{J} \times \mathbf{B} - \nabla p_e), \end{aligned} \quad (5)$$

where  $\mathbb{P}$  is the anisotropic plasma pressure and  $p_e$  is the electron pressure. The other symbols have their usual meanings. Various electron and ion parameters and the single-fluid quantities are given by

$$n_i \simeq n_e \equiv N, \quad (6)$$

$$\rho = n_i m_i + n_e m_e \approx N(m_i + m_e) \simeq N m_i, \quad (7)$$

$$\mathbf{v} = \frac{1}{\rho} (n_i m_i \mathbf{v}_i + n_e m_e \mathbf{v}_e) \approx \frac{m_i \mathbf{v}_i + m_e \mathbf{v}_e}{m_i + m_e} \simeq \mathbf{v}_i, \quad (8)$$

$$\mathbf{J} = e(n_i \mathbf{v}_i - n_e \mathbf{v}_e) \approx eN(\mathbf{v}_i - \mathbf{v}_e), \quad (9)$$

$$\mathbb{P} = p_\perp \delta_{ij} + (p_\parallel - p_\perp) \hat{b}_i \hat{b}_j. \quad (10)$$

The unit vectors  $\hat{b}_i$  are the components of the magnetic field vector ( $\mathbf{B}/B$ ). For plasma pressure, we use Stasiewicz's polybaric pressure equations [18]

$$p_\perp = p_{\perp 0} \left( \frac{N}{N_0} \right)^\gamma \left( \frac{B}{B_0} \right)^\kappa, \quad (11)$$

$$p_\parallel = p_\perp (a_p + 1), \quad (12)$$

where

$$a_p = p_\parallel / p_\perp - 1 \quad (13)$$

is the pressure anisotropy parameter, which is assumed to be constant. It should be noted here that this pressure model belongs to a more general class of polybaric pressure model with variable anisotropy

$$a_p = p_\parallel / p_\perp = a_{p0} \left( \frac{N}{N_0} \right)^{\gamma_a} \left( \frac{B}{B_0} \right)^{\kappa_a}, \quad (14)$$

where  $(\gamma_a, \kappa_a)$  are the anisotropy indices. This model has been successfully applied to various magnetosonic oscillations in different regions of magnetosphere with  $0.5 < \gamma < 2$  and  $\kappa$  ranging from 0 to  $-2$ . These pressure equations provide

TABLE I. Plasma parameters for the event shown in Fig. 4(a).

Alfvén velocity	$V_A \approx 100$ km/s
Ion inertial length	$\lambda_i \approx 40$ km
Plasma $\beta$	$\beta \approx 20$
Electron $\beta$	$\beta_e \approx 0.3$
Plasma (ion) velocity	$V_i = (-60, 0, -110)$ km/s
Structure velocity (magnitude)	$U = -48$ km/s
Direction normal	$\hat{n} = (0.853, -0.288, 0.436)$

an effective approximation for the observed data for magnetospheric plasma boundaries and can model various types of particle-field energy exchange [18]. In MHD, simplified expressions for anisotropic pressure can be obtained by assuming a small ion gyroradius (compared to the scale of the plasma), so that the perpendicular velocity can be effectively controlled by the adiabatic invariant  $\mu$  [19] resulting in a reduction of kinetic variables in the guiding center Vlasov theory, and the pressure expressions become

$$p_\perp = \frac{1}{2} m_i \int f_i u_\perp^2 d\mathbf{u}, \quad (15)$$

$$p_\parallel = m_i \int f_i (u_\parallel - \mathbf{v} \cdot \hat{\mathbf{b}}) d\mathbf{u}. \quad (16)$$

The CGL double adiabatic equations are the result of the above expressions with the assumptions that the system must evolve very slowly, so that  $u_\perp^2 \propto \mu B$  is entirely determined by the adiabatic invariant  $\mu$ , resulting in  $p_\perp \propto N v_\perp^2 \propto N B$ . However, when the FLR effects become important, one cannot ensure the invariance of  $\mu$ , and the approximations leading to CGL equations break down. This is what exactly happens in the magnetopause region as the observed data do not conform to the CGL theory, but rather obey a more general polybaric pressure equations such as given in Eqs. (11) and (12). The fact that the perpendicular pressure  $p_\perp \propto N^\gamma B^\kappa$  signifies that  $\mu \propto v_\perp^2 / B$  is no longer an adiabatic invariant. Besides, we also note that in CGL-type models, the anisotropy parameter  $a_p$  is not a constant. This, however, requires that the magnetic field  $B$  should depend on density rather strongly, which is not supported by observational data, at least in the magnetopause region [12]. So, it is sensible to assume that the kinetic effects keep the anisotropy at a constant level. This also simplifies our physical model, though a variable anisotropy can very well be treated in the present framework, which, however, will make the analytical treatment of the underlying dynamical model impossible.

As the measured average plasma pressure (the ion pressure) in the magnetopause region is about 70–100 times more than the electron pressure (see Table I), the anisotropy in electron pressure is not expected to play a significant role and is assumed to be isotropic, although a more general anisotropic electron pressure will not change the general outcome of the analysis:

$$p_e = p_{e0} \left( \frac{N}{N_0} \right) \left( \frac{T}{T_0} \right). \quad (17)$$



The quantities with subscript “0” denote their corresponding values at equilibrium. The above equations are closed by Maxwell’s equations:

$$\nabla \times \mathbf{B} = \mu_0 \mathbf{J}, \quad (18)$$

$$\nabla \times \mathbf{E} = -\frac{\partial \mathbf{B}}{\partial t}, \quad (19)$$

$$\nabla \cdot \mathbf{B} = 0. \quad (20)$$

In what follows, as the temperature remains constant, we absorb it in the definition of  $p_{e0}$ .

### III. PERTURBATION AND REDUCTION

We now consider a general electromagnetic perturbation of the system in a frame moving with the wave in the  $x$  direction, so that with respect to the wave, we have  $\partial/\partial t \equiv 0$ . All other quantities are assumed to be dependent on  $x$ , so that  $\partial/\partial y \equiv \partial/\partial z \equiv 0$ . The equilibrium magnetic field is assumed to be in the  $x$ - $z$  plane ( $B_{0y} = 0$ ),

$$\mathbf{B}_0 = \hat{x} B_0 \cos \alpha + \hat{z} B_0 \sin \alpha, \quad (21)$$

at an angle  $\alpha$  to the  $x$  direction. The equilibrium flow velocity is also assumed to be in  $x$  direction,  $\mathbf{v} = v_0 \hat{x}$ . Far from the perturbation at  $x \rightarrow \infty$ , the plasma density  $N = N_0$ , the equilibrium density. Note that at  $\infty$  the flow velocity becomes the equilibrium velocity.

From the time-independent continuity equation, we now have

$$N v_x = N_0 v_0 = \text{const.} \quad (22)$$

Faraday’s law implies that

$$\nabla \times \mathbf{E} = 0, \quad (23)$$

from which we get  $E_y = E_z = \text{const.}$  The divergence-free magnetic field implies that  $B_x = B_{x0} = \text{const.}$  From Ampère’s law, we have

$$\mathbf{J} = \frac{1}{\mu_0} \nabla \times \mathbf{B}. \quad (24)$$

We now normalize the density by its equilibrium value,  $n \rightarrow N/N_0$  and define the normalized velocity as  $M_A = v_0/v_A$ , which is the Alfvén Mach number, and the Alfvén velocity  $v_A$  is given as

$$v_A = \sqrt{\frac{B_0^2}{\mu_0 N_0 m_i}}. \quad (25)$$

The plasma  $\beta$  is defined as the ratio of the plasma pressure (perpendicular) to the magnetic pressure at equilibrium state:

$$\beta = \frac{p_{\perp 0}}{B_0^2/(2\mu_0)}. \quad (26)$$

Note that through Eq. (22), we have  $v_0/v_x = n$ , where  $n$  is the dimensionless density. We further define the normalized magnetic field as  $\mathbf{b} = \mathbf{B}/B_0$  with  $b_x \equiv b_{x0} = \text{const}$  and  $b_0 \equiv 1$ .

The  $x$  component of the momentum equation, Eq. (4) can now be written as

$$N m_i v_x \frac{\partial v_x}{\partial x} = -\frac{1}{2\mu_0} \frac{\partial}{\partial x} (B_y^2 + B_z^2) - \frac{\partial}{\partial x} \mathbb{P}_{xx}, \quad (27)$$

where

$$\mathbb{P}_{xx} = p_{\perp} + (p_{\parallel} - p_{\perp}) \frac{b_x}{b}. \quad (28)$$

Integrating Eq. (27), we have

$$N m_i v_x^2 = -\frac{1}{2\mu_0} (B_y^2 + B_z^2) - \mathbb{P}_{xx} + C, \quad (29)$$

where we have utilized the condition that  $N v_x = \text{const}$  and  $C$  is the integration constant, which is evaluated by imposing the boundary conditions at  $x \rightarrow \infty$ ,

$$C = N_0 m_i v_0^2 + \frac{1}{2\mu_0} (B_{y0}^2 + B_{z0}^2) + \mathbb{P}_{xx0}, \quad (30)$$

where

$$\mathbb{P}_{xx0} = p_{\perp 0} + (p_{\parallel 0} - p_{\perp 0}) b_{x0}^2. \quad (31)$$

With these expressions, Eq. (29) can be expressed as

$$2M_A^2(n^{-1}-1) + \beta(n^\gamma b^\kappa - 1) + b^2 - 1 + b_{x0}^2 a_p \beta(n^\gamma b^{\kappa-2} - 1) = 0. \quad (32)$$

The transverse components (i.e.,  $y$  and  $z$  components) of Ohm’s law (5) are respectively given by

$$\frac{1}{eN\mu_0} B_{x0} \frac{\partial B_y}{\partial x} = E_y + v_z B_{x0} - v_x B_z - \frac{1}{eN} \frac{\partial p_e}{\partial x}, \quad (33)$$

$$\frac{1}{eN\mu_0} B_{x0} \frac{\partial B_z}{\partial x} = E_z + v_x B_y - v_y B_{x0}. \quad (34)$$

In equilibrium (or at  $x \rightarrow \infty$ ), Ohm’s law (5) can be written as

$$\mathbf{E}_0 + \mathbf{v}_0 \times \mathbf{B}_0 = -\frac{1}{eN_0} \nabla p_{e0} \quad (35)$$

as the equilibrium current density vanishes. The transverse components of the above equation yield

$$E_y \equiv E_{y0} = v_{x0} B_{z0}, \quad (36)$$

$$E_z = E_{z0} = 0. \quad (37)$$

From the transverse components of the momentum equation, we have

$$N m_i v_x \frac{\partial v_y}{\partial x} = \frac{1}{\mu_0} B_{x0} \frac{\partial B_y}{\partial x} - \frac{\partial}{\partial x} \mathbb{P}_{xy}, \quad (38)$$

$$N m_i v_x \frac{\partial v_z}{\partial x} = \frac{1}{\mu_0} B_{x0} \frac{\partial B_z}{\partial x} - \frac{\partial}{\partial x} \mathbb{P}_{xz}. \quad (39)$$

Integrating the above equations and evaluating the corresponding integration constants at  $\infty$ , we can solve for  $v_{y,z}$  as

$$v_y = \frac{1}{m_i N v_x \mu_0} (B_{x0} B_y - \mu_0 \mathbb{P}_{xy}), \quad (40)$$

$$v_z = \frac{1}{m_i N v_x \mu_0} [B_{x0} (B_z - B_{z0}) - \mu_0 (\mathbb{P}_{xz} - \mathbb{P}_{xz0})]. \quad (41)$$



We note that

$$\mathbb{P}_{xy} = (p_{\parallel} - p_{\perp}) \frac{b_x}{b} \frac{b_y}{b}, \quad (42)$$

$$\mathbb{P}_{xz} = (p_{\parallel} - p_{\perp}) \frac{b_x}{b} \frac{b_z}{b}, \quad (43)$$

from which we can see that

$$\mathbb{P}_{xy0} = 0, \quad \mathbb{P}_{xz0} = (p_{\parallel 0} - p_{\perp 0}) b_{x0} b_{z0}. \quad (44)$$

Using Eqs. (40)–(44) in Eqs. (33) and (34), we can finally write

$$\begin{aligned} \frac{1}{M_x} \frac{\partial b_y}{\partial x} &= b_{z0} \left[ n - \frac{n}{M_x^2} \left( 1 - \frac{1}{2} a_p \beta \right) \right] \\ &\quad - b_z \left[ 1 - \frac{n}{M_x^2} \left( 1 - \frac{1}{2} a_p \beta n^{\gamma} b^{\kappa-2} \right) \right] \\ &\quad - \beta_e \frac{1}{2M_A} \frac{\partial n}{\partial x}, \end{aligned} \quad (45)$$

$$\frac{1}{M_x} \frac{\partial b_z}{\partial x} = b_y \left[ 1 - \frac{n}{M_x^2} \left( 1 - \frac{1}{2} a_p \beta n^{\gamma} b^{\kappa-2} \right) \right], \quad (46)$$

where  $M_x = M_A/b_{x0}$ , and the length  $x$  is normalized by the inertial ion length  $\lambda_i = v_A/\omega_{ci}$  with  $\omega_{ci} = eB_0/m_i$  as the ion gyro-frequency. The FLR effects are incorporated to the above model through  $\beta_e$ , the ratio of electron pressure to the magnetic pressure

$$\beta_e = \frac{p_{e0}}{B_0^2/(2\mu_0)}. \quad (47)$$

When  $\beta_e \rightarrow 0$ , we recover Stasiewicz's equations [12]. The above coupled differential equations can be termed as structure equations of the system that describes the flow of plasma.

#### IV. DYNAMICAL ANALYSIS

We now consider the possible oscillations of  $b_{y,z}$  in space as determined by Eqs. (45)–(46). Consider the dynamical model represented by these equations but without the FLR effect, which reduces the model to

$$\begin{aligned} \frac{1}{M_x} \frac{\partial b_y}{\partial x} &= b_{z0} \left[ n - \frac{n}{M_x^2} \left( 1 - \frac{1}{2} a_p \beta \right) \right] \\ &\quad - b_z \left[ 1 - \frac{n}{M_x^2} \left( 1 - \frac{1}{2} a_p \beta n^{\gamma} b^{\kappa-2} \right) \right] \\ &\equiv f(b_y, b_z), \end{aligned} \quad (48)$$

$$\begin{aligned} \frac{1}{M_x} \frac{\partial b_z}{\partial x} &= b_y \left[ 1 - \frac{n}{M_x^2} \left( 1 - \frac{1}{2} a_p \beta n^{\gamma} b^{\kappa-2} \right) \right] \\ &\equiv g(b_y, b_z). \end{aligned} \quad (49)$$

The equilibrium points of the above dynamical system are given by the condition  $\partial b_{y,z}/\partial x = 0$ . We note that the functions  $f$  and  $g$  can be expressed entirely in terms of  $b_{y,z}$ , as  $n$  can be expressed in terms of  $b_{y,z}$  by Eq. (32). We can see from Eq. (49) that  $g(b_y, b_z) = 0$  requires either of the following

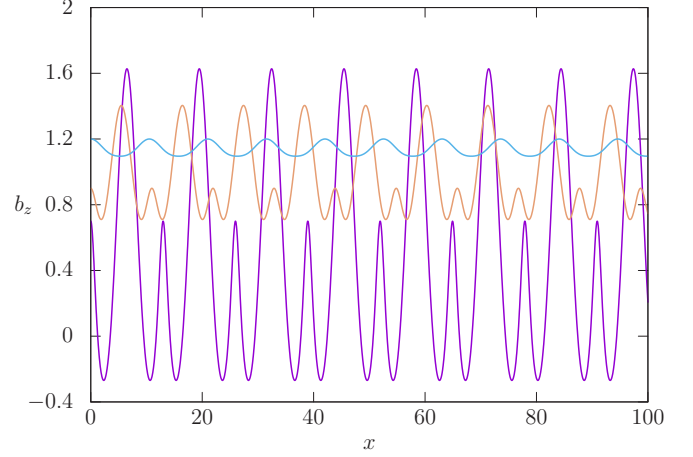


FIG. 1. Oscillations in  $b_z$  without the FLR effect. The initial points, respectively, for the largest to the smallest amplitudes are  $(b_y, b_z) = (0, 0.7)$ ,  $(0, 0.9)$ , and  $(0, 1.2)$ .

conditions to be satisfied:

$$\begin{aligned} b_y &= 0 \\ \frac{n}{M_x^2} \left( 1 - \frac{1}{2} a_p \beta n^{\gamma} b^{\kappa-2} \right) &= 1. \end{aligned} \quad (50)$$

Surely, the second condition is too restrictive and cannot be maintained for all values of  $n$ ,  $\beta$ ,  $a_p$ ,  $\gamma$ ,  $\kappa$ ,  $M_x$ , and  $b$  and has to be discarded as a possible solution, which leaves the only feasible condition for equilibrium as  $(b_y, b_z) = (0, b_z^*)$ , where  $b_z^* (\neq 0)$  is to be determined. A linearization of the system around this equilibrium point yields the following Jacobian [20]:

$$J = \begin{pmatrix} \partial f / \partial b_y & \partial f / \partial b_z \\ \partial g / \partial b_y & \partial g / \partial b_z \end{pmatrix}_{(0, b_z^*)} = \begin{pmatrix} 0 & f_z \\ g_y & 0 \end{pmatrix}, \quad (51)$$

where  $f_z, g_y$  are nonzero functions of  $b_z^*$ . We recall that the behavior of a nonlinear dynamical model can be inferred pretty accurately in the vicinity of the equilibrium points from the behavior of the corresponding linearized system [20]. The key to the behavior of the linearized model lies in the trace ( $\tau$ ) and determinant ( $\Delta$ ) of the corresponding Jacobian  $J$ ; the unstable and stable orbits lie on the either side of the parabola defined by the equation

$$\tau^2 - 4\Delta = 0 \quad (52)$$

in the  $\Delta$ - $\tau$  plane [20]. For unstable orbits, we need ( $\Delta > 0$ ,  $\tau > 0$ ) while stable orbits require ( $\Delta > 0$ ,  $\tau < 0$ ). We have saddle points for  $\Delta < 0$ . If we have  $\Delta > 0$  and  $\tau = 0$ , we have what is known as *centers*, defined by a set of infinite number of periodic orbits for different initial points in the phase plane  $(b_y, b_z)$  [20]. It is now obvious from Eq. (51) that we have a set of an infinite number of periodic orbits for the dynamical system represented by Eqs. (48) and (49) for different initial points in the phase plane  $(b_y, b_z)$ , as determined by the trace (which is zero). This situation is physically not favorable as different initial points in the  $(b_y, b_z)$  plane push the solution of Eqs. (48) and (49) into different periodic orbits which may have arbitrarily small or large amplitudes, whereas practically



we do not see oscillations with such arbitrary amplitudes. A few such oscillations are shown in Fig. 1, which are generated with different initial points.

### A. FLR effect

We now linearize our dynamical equations about the equilibrium point  $(b_y, b_z) = (0, b_z^*)$  with the FLR term taken into account [Eqs. (45) and (46)]. Note that these equations involve

both  $n$  and  $\partial n / \partial x$ , which need to be expressed in terms of  $b_{y,z}$  and  $b'_{y,z}$  before Eqs. (45) and (46) can be solved.

Both  $n$  and  $\partial n / \partial x$  can be expressed in terms of  $b_{y,z}$  using Eqs. (27) and (32). We note that Eq. (32) is an algebraic equation which admits more than one solution of  $n$ . In order to see which solution is viable, we simplify the mathematics by assuming  $\gamma \sim 1$  (which is very close to the adiabatic value of 5/3). This transforms Eq. (32) to a quadratic equation in  $n$ , of which we choose the solution by applying the boundary conditions at  $x \rightarrow \infty$ , when  $b \rightarrow 1$  and  $n \rightarrow 1$ :

$$n = 4M_A^2 b^2 [b^2(1 + 2M_A^2 + \beta + a_p \beta b_{x0}^2) - b^4 - \{b^4(1 - b^2 + 2M_A^2 + \beta + a_p \beta b_{x0}^2)^2 - 8b^{2+\kappa} \beta M_A^2 (b^2 + a_p b_{x0}^2)\}^{1/2}]^{-1}, \quad (53)$$

$$\frac{\partial n}{\partial x} = \frac{2n^2 + \beta b^{\kappa-4} n^3 (a_p b_{x0}^2 (\kappa - 2) + b^2 \kappa)}{2M_A^2 - \beta b^{\kappa-2} n^2 (a_p b_{x0}^2 + b^2)} \frac{\partial b}{\partial x}. \quad (54)$$

The particular solution for  $n$  is fixed from the boundary conditions that at  $\infty$ ,  $b \rightarrow 1$  and  $n \rightarrow 1$ . Note that the equilibrium points of Eqs. (45) and (46) remain the same as before and are not affected by the inclusion of the FLR term. As noted before, the stability of the equilibrium points is determined by the form of the Jacobian  $J$ . The trace of the linearized Jacobian for arbitrary  $\kappa$  can be written as

$$\text{Tr}(J) = \frac{\beta_e n_\star^3}{4M_A^2 b_\star^2} \left( \frac{b_{z0}}{b_{x0}} \right) \frac{[2M_A^2 + b_{x0}^2 (a_p \beta - 2)] [\beta b_\star^\kappa n_\star \{ \kappa + a_p b_{x0}^2 (\kappa - 2) / b_\star^2 \} + 2b_\star^2]}{[\beta b_\star^\kappa n_\star^2 (1 + a_p b_{x0}^2 / b_\star^2) - 2M_A^2]}, \quad (55)$$

which reduces to the following expression for  $\kappa = 0$ :

$$\text{Tr}(J)|_{\kappa=0} = \frac{\beta_e n_\star^3}{2M_A^2 b_\star^2} \left( \frac{b_{z0}}{b_{x0}} \right) \frac{(b_\star^2 - a_p \beta n_\star b_{x0}^2 / b_\star^2) [2M_A^2 + b_{x0}^2 (a_p \beta - 2)]}{[\beta n_\star^2 (1 + a_p b_{x0}^2 / b_\star^2) - 2M_A^2]}, \quad (56)$$

where  $(n_\star, b_\star) = (n, b)|_{(0, b_z^*)}$ . A reduction, say for the positivity condition for the trace,  $\text{Tr}(J) > 0$  from expression (55) yields any of the following groups of conditions to be satisfied simultaneously:

$$\begin{aligned} a_p &< 0, \quad |a_p| > \frac{b_{x0}^2}{b_\star^2}, & a_p &< 0, \quad |a_p| < \frac{b_{x0}^2}{b_\star^2}, \\ M_A &< |b_{x0}| \left( 1 - \frac{1}{2} a_p \beta \right)^{1/2}, & \text{or } M_A &\geq |b_{x0}| \left( 1 - \frac{1}{2} a_p \beta \right)^{1/2}, \\ n_\star^{1+\gamma} &\geq \frac{2M_A^2}{\beta b_\star^\kappa} \left( 1 + a_p \frac{b_{x0}^2}{b_\star^2} \right)^{-1}, & n_\star^{1+\gamma} &\geq \frac{2M_A^2}{\beta b_\star^\kappa} \left( 1 + a_p \frac{b_{x0}^2}{b_\star^2} \right)^{-1}, \end{aligned} \quad (57)$$

with the assumption that  $\kappa < 0$ . We note that experimental observations fix  $\kappa$  within a probable range of  $-2$  and  $0$  [18]. Within a probable set of realistic physical parameters, all of the above conditions can be satisfied so that  $\text{Tr}(J)$  can be either made positive or negative resulting in unstable and stable oscillations. It is worth noting that we do not have an infinite set of periodic orbits. These equations exhibit a wide variety of dynamical variations, which we describe in the next section.

### B. Bifurcations and stability: Nonexistence of limit cycle

In order to examine the bifurcations of the dynamical model, we rely on the physical data from various satellite-based experiments from the magnetopause region of the earth's magnetosphere where the FLR effects are supposed to be dominant. In what follows, all the sets of data that are used are from the *Cluster* data repository. As an example, we consider the stability of the equilibrium points of Eqs. (48)

and (49) for  $\kappa = 0$ . The behavior of the dynamical model for nonzero  $\kappa$  is shown in Sec. V when we compare our results with observations.

We now prove that this system does not possess a limit cycle. We note, however, that this conclusion of ours cannot be rigorously proved mathematically, owing to the complexity of the system (see below the conjectures). A limit cycle is an isolated and stable periodic orbit of a nonlinear dynamical system, so that all nearby trajectories are attracted to the limit cycle, and irrespective of any perturbations, the oscillations always tend to settle down on the limit cycle [20]. Physically, a limit cycle behavior indicates a reproducible and consistent periodic oscillations of a dynamical system and indicates the fundamental oscillatory behavior of the system. Mathematically, existence of a limit cycle indicates presence of self-consistent stable oscillations as a fundamental behavior of the underlying physical system. In this case, however, this does not happen. It is worth noting here that a solid analytical mathematical proof for nonexistence of a limit cycle in a



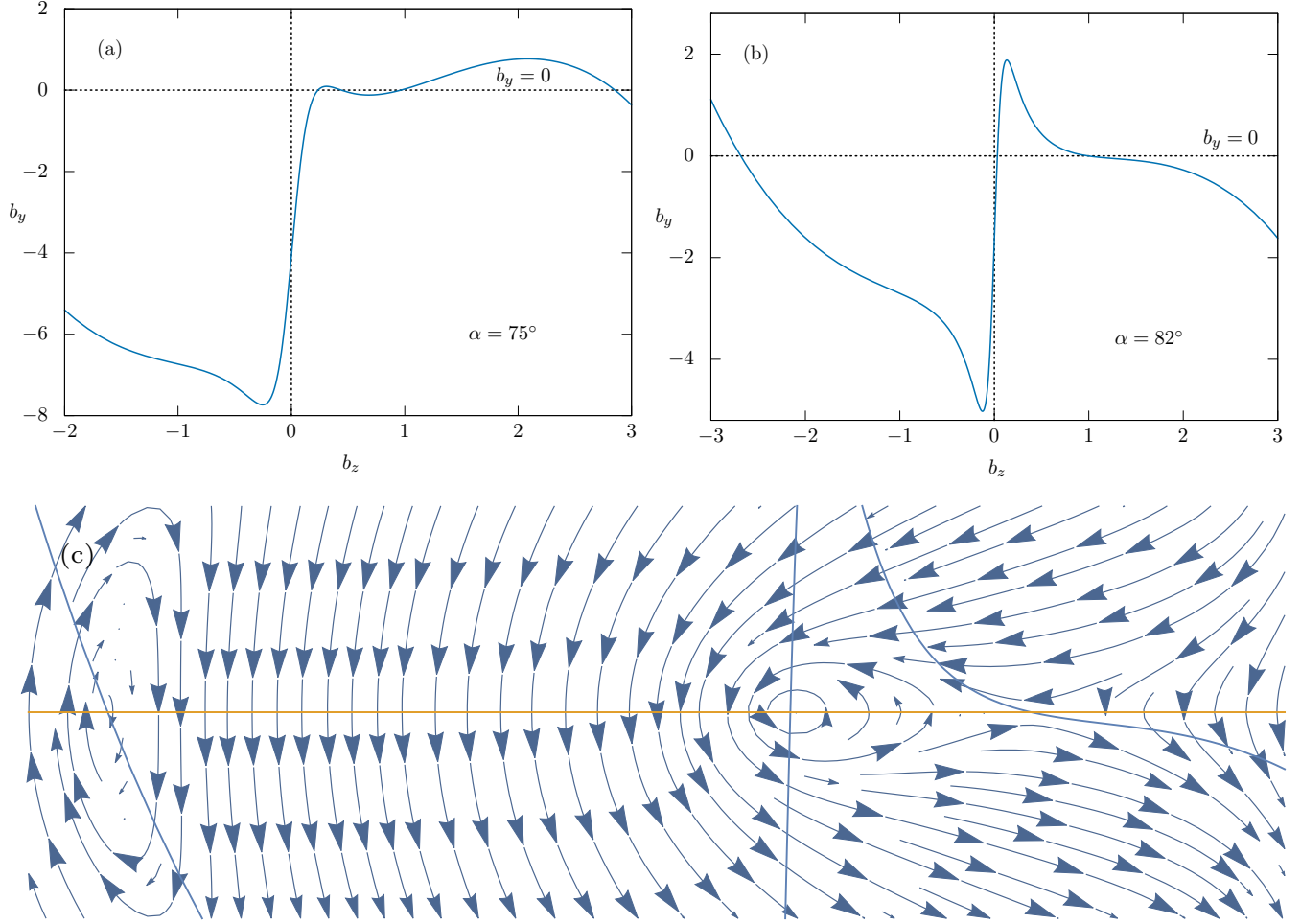


FIG. 2. Nullclines (a), (b) of Eqs. (45) and (46) in the  $(b_y, b_z)$  plane for different values of  $\alpha$  showing the equilibrium points of the system (the intersections of  $b_z$  with the  $b_y = 0$  line). (c) The position of the equilibrium points are shown with the stream plot of the flow in the  $(b_y, b_z)$  plane for the case  $\alpha = 82^\circ$ . The three intersections of the flows with the central horizontal line indicates the corresponding equilibrium points.

region  $\mathcal{R}$ , rather than existence, is a potentially difficult issue, especially for a complex system like the one as described by Eqs. (45) and (46). So we adopt a three-pronged strategy to prove our conjecture.

Consider now a set of probable but arbitrary physical parameters as  $\beta = 10$ ,  $\alpha = 82$ ,  $a_p = -0.1$ , and  $\beta_e = 0.2$ . Note that the value of  $\beta_e$  does not affect the behavior of the equilibrium points. For  $M_A = 0.1$ , the system has three equilibrium points at  $(b_y, b_z) = (0, -2.685)$ ,  $(0, 0.032)$ , and  $(0, 0.99)$ , among which the first two are stable sinks (an inward spiraling orbit) and the third one is a saddle point. So depending on the initial starting value, the solution of the equations always goes away from the stable periodic orbit (when the FLR effects were absent), and the oscillations always decay and spiral down to settle down on one of the sinks. If we now increase the value of  $M_A$  to 0.2, we observe a complete change of behavior of the equilibrium points. The equilibrium points are now  $(b_y, b_z) = (0, -0.495)$ ,  $(0, -0.0185)$ , and  $(0, 0.99)$ . The first one now has become a saddle point, while the last two points are now unstable sources (an outward-spiraling orbit). It is interesting to note that the third point, the value of which does not depend on  $M_A$ , changes its behavior. So

a supercritical Hopf bifurcation occurs at  $b_z \approx 0$ , which can also be degenerate [21]. In Fig. 2 we show this behavior with the parameter  $\alpha$ .

Note that when a supercritical degenerate Hopf bifurcation occurs, the dynamical system, following the bifurcation, may show multiple limit cycles (closed and isolated periodic orbits) or may have a limit cycle at  $\infty$ . The first one is generally called a *supercritical degenerate Hopf bifurcation of the first kind*, and the second one is called a *supercritical degenerate Hopf bifurcation of the second kind* [21]. In our case, the numerical phase portrait show that our system (45) and (46) may undergo a supercritical degenerate Hopf bifurcation of the second kind (see Fig. 3). It can be noted here that the existence of a supercritical Hopf bifurcation is not limited to any specific set of parameters such as  $\kappa = 0$ . As we show in Fig. 3(b), a similar bifurcation occurs even for  $\kappa \neq 0$ .

### 1. The numerically calculated phase portrait

We note that when the dynamical system is analytically not treatable, a numerically calculated phase portrait can indicate the overall flow behavior of the system for the relevant



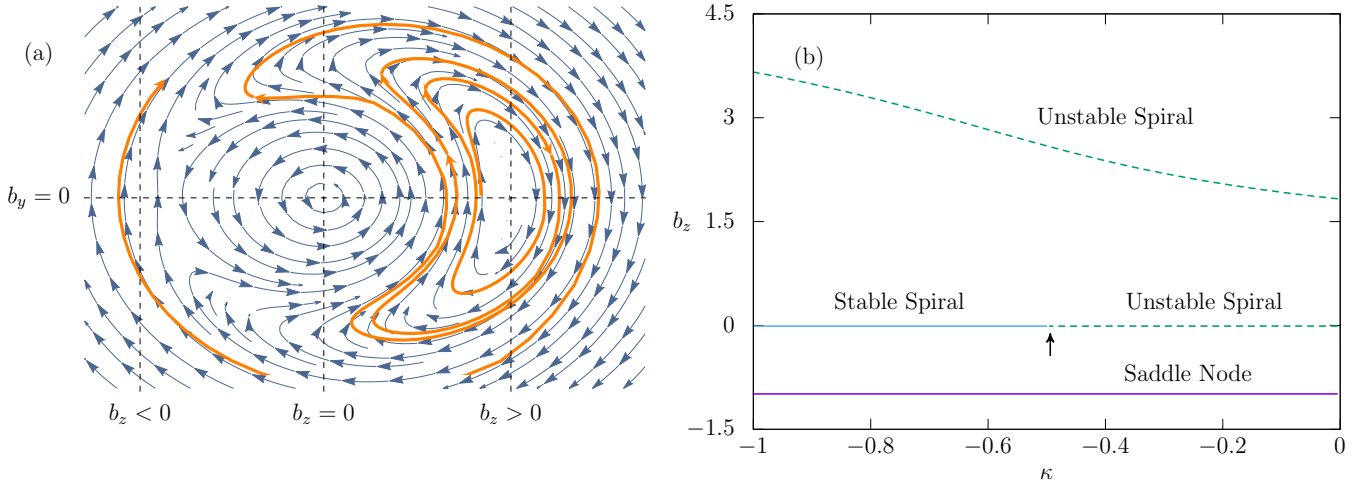


FIG. 3. (a) The stream plot of Eqs. (45) and (46) in the  $b_z$ - $b_y$  plane is shown for a realistic parameter set. The solid line shows the overall flow pattern. (b) The progression of behaviors of the equilibrium points of Eqs. (45)–(46) for the same set of parameters (see Sec. V) in the  $(\kappa$ - $b_z$ ) plane. The arrow indicates the Hopf bifurcation point.

parameter regime. In Fig. 3(a) we have shown the stream plot of the flow vectors of Eqs. (45) and (46) in the realistic parameter regime. The Hopf bifurcation occurs near  $b_z = 0$  and the oscillations of interest begin around the point indicated by  $b_z > 0$ . The solid orange line shows the overall flow behavior. As can be seen, the oscillation begins around  $b_z > 0$  and increases in amplitude until it is caught by the unstable spiral, created at  $b_z \simeq 0$  following the Hopf bifurcation. The flow then goes away from the unstable equilibrium point to infinity, and the orbits may converge at  $\infty$  (which, however, cannot be proved rigorously). So our first conjecture is the following:

*Conjecture 1:* In the physically relevant parameter regime of  $b_z > 0$ , the system represented by Eqs. (45) and (46) does not seem to have any stable closed orbit until  $(b_y, b_z)$  becomes very large.

## 2. Bendixson-Dulac criterion

The Bendixson-Dulac criterion [22–24] state that for any two functions  $f(x, y)$ ,  $g(x, y)$  with continuous and simply connected derivatives  $\partial f/\partial x$  and  $\partial g/\partial y$  in a region  $\mathcal{R}$ , if we can find an arbitrary function  $\phi(x, y)$  such that

$$\mathcal{D}(x, y) \equiv \frac{\partial}{\partial x}(\phi f) + \frac{\partial}{\partial y}(\phi g) \neq 0 \text{ in } \mathcal{R}, \quad (58)$$

then the system

$$\begin{aligned} x' &= f(x, y) \\ y' &= g(x, y) \end{aligned} \quad (59)$$

does not possess any closed orbit in  $\mathcal{R}$ . We note, however, that the Bendixson-Dulac criteria do not indicate what happens when  $\mathcal{D}(x, y) = 0$ . For the system Eqs. (45) and (46), however the equivalent function  $\mathcal{D}(b_y, b_z)$  is too complex to be reduced algebraically and the criteria to be proved analytically. So, we consider its asymptotic behavior at  $(b_y, b_z) \rightarrow \infty$

choosing  $\phi(x, y) = 1$ ,

$$\mathcal{D}(b_y, b_z)|_{b_y, b_z \rightarrow \infty} \simeq 4M_A \frac{b_{z0}}{b_{x0}} \left( \frac{b_y}{b_z^4} + \frac{1}{b_y^4} \right) \left[ M_A^2 + b_{x0}^2 \left( \frac{1}{2} a_p \beta - 1 \right) \right], \quad (60)$$

and we see that

$$\lim_{b_y, b_z \rightarrow \infty} \mathcal{D}(b_y, b_z) = 0,$$

which leads to the second conjecture.

*Conjecture 2:* The system represented by Eqs. (45) and (46) can possess a closed orbit at  $\infty$  in the  $(b_y, b_z)$  space, thus supporting the first conjecture.

It should be noted that through the Bendixson-Dulac criteria, we cannot rule out the nonexistence of closed orbit in the finite  $(b_y, b_z)$  plane.

## 3. The index theory

As per index theory [25], we know that the index of a closed trajectory of a two-dimensional planar system indicates the global behavior of its trajectories. As shown in Fig. 3(a), the indices  $I_C$  of the fixed points at  $b_z > 0$ ,  $b_z = 0$ , and  $b_z < 0$  are, respectively, +1, +1, and -1, of which the first two are sources and the last one is a saddle point. From the phase portrait, we see that closed trajectories (a limit cycle) around the first two fixed points are not possible because the trajectories around the first fixed point are carried away by the trajectories of the second and the trajectories of the second one are swept by the third one, which is a saddle point. A closed orbit is also not possible enclosing the first two fixed points because the indices of both add to +2, but a closed orbit must have an index of +1, according to the theory of index. If there is any closed orbit in the  $b_y$ - $b_z$  plane, it must enclose all the three fixed points as the indices of all three add to +1. However, this requires  $b_z$  to be necessarily oscillating around



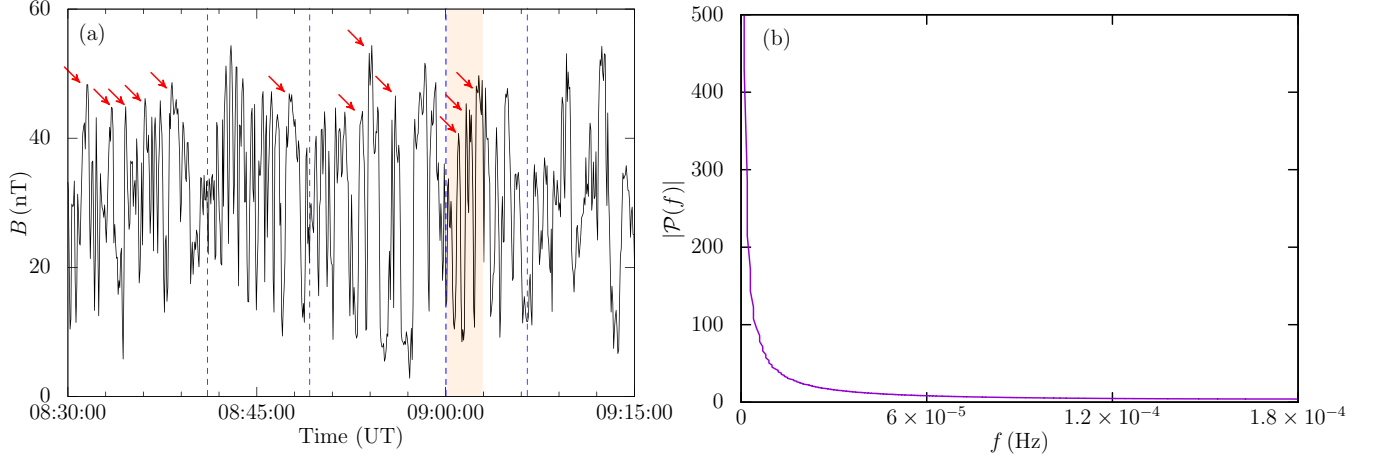


FIG. 4. Oscillations of the geomagnetic field  $B$  as detected by *Cluster* spacecraft 1 on February 3, 2002 (a) between 08:30:00 and 09:15:00 hours (UT). The dashed lines indicate the divisions of groups of solitons, and the arrows indicate few individual solitons. (b) The plot of the corresponding power spectrum density  $\mathcal{P}(f)$  of these oscillations, plotted against the sampling frequency  $f$ , which shows no detectable linear wave train.

$b_z = 0$ , which does not fall in the parameter regime of interest. This leads us to the final and third conjecture:

**Conjecture 3:** The system represented by Eqs. (45) and (46) cannot have any closed orbit around a fixed point in the region where  $b_z \geq 0$ , and if there is any closed orbit, it must be at  $b_{y,z} \rightarrow \infty$ .

So, from these three conjectures, we can finally conclude that the system represented by Eqs. (45) and (46) does not have a closed periodic orbit (i.e., a limit cycle) in the finite region of interest where  $b_z > 0$ . All these analyses indicate that the system undergoes a supercritical degenerate Hopf bifurcation of the second kind at  $b_z = 0$ .

## V. NUMERICAL RESULTS AND OBSERVATIONS

In this section, we put forward our analysis of unstable (or stable) oscillations in the perspective of experimental observations, namely, observations by the fleet of *Cluster* spacecrafts. In Fig. 4 we show a section of such oscillations, which was observed by *Cluster* spacecraft 1 on February 3, 2002, in the magnetopause region. We emphasize that these

oscillations do not indicate existence of any periodicity, which is confirmed by the power spectrum analysis shown alongside in Fig. 4(b), where the value of spectral density  $\mathcal{P}(f)$  does not show any periodicity for any frequency  $f$ . This is a strong indication that these oscillations are *groups* of train of solitary waves generated nonlinearly in the magnetopause region. We have indicated a few such soliton peaks with arrows in the figure. An inspection of these oscillations also reveals the existence of several such groups of solitons (indicated by the dashed vertical lines in the figure), with progressively increasing magnitudes. We also note here that modeling these groups of solitons requires  $|\kappa| \sim 0$  as higher values of  $\kappa$  cause the oscillations to die (see Fig. 3). Our test case is the train of solitons shown in the shaded region from 08:59:00 and 09:03:00 hours. The plasma parameters as detected by the spacecraft are given in Table I and in Fig. 5. The measurements of different parameters (as observed by the spacecrafts) are given in the Geocentric Solar Ecliptic (GSE) coordinate. The actual position of the *Cluster* fleet during the event in question is shown in Fig. 6, reproduced in scale with the help of NASA's 4D Orbit Viewer. As can be seen, during 08:00:00

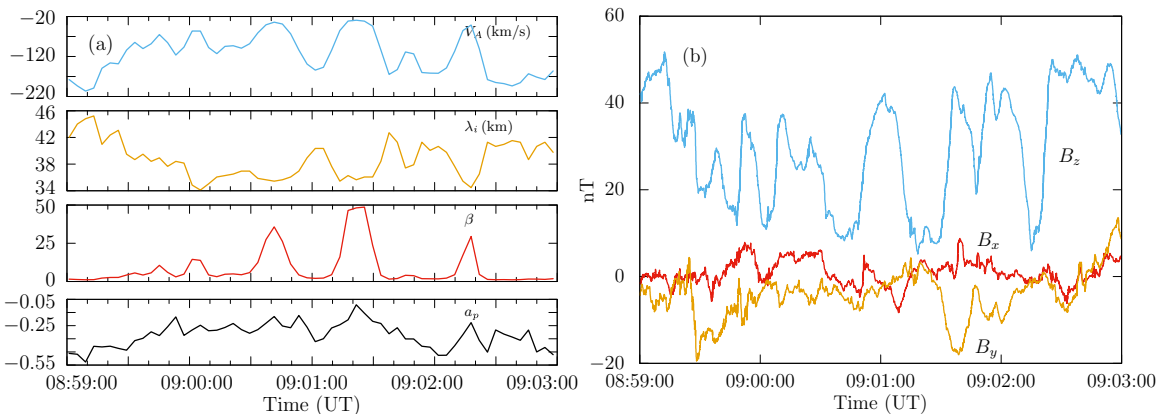


FIG. 5. (a) Alfvén velocity  $V_A$ , ion inertial length,  $\lambda_i$  plasma  $\beta$ , and pressure anisotropic parameter  $a_p$  as detected by *Cluster* spacecraft 1 corresponding to the event shown in Fig. 4(a). (b) The field variation after an MVA analysis.



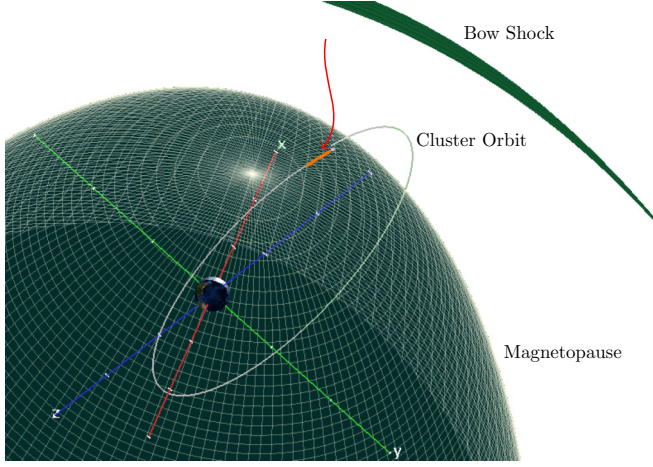


FIG. 6. Position of the *Cluster* spacecrafts between 08:00:00 and 09:00:00 hours (UT) on February 3, 2002, as shown by the red arrow (reproduced in scale with the help of NASA's 4D Orbit Viewer). The figure is drawn with earth at the center in the GSE coordinates.

and 09:00:00 hours (UT), the *Cluster* fleet was just crossing the magnetopause, where we expect to see the effect of FLR on the solitary oscillations.

The pressure anisotropy parameter  $a_p$  is determined from the ion temperature data measured by the Cluster Ion Spectrometer (CIS) [26]. The CIS data also determine the plasma velocity (as measured from ion flow data)  $V_i = (-60, 0, -110)$  km/s. From a time-shift measurement of the four *Cluster* spacecrafts, the velocity of the nonlinear structure can be determined as  $U = (-40, 13.8, -20)$  km/s. This determines the structure velocity with respect to the plasma along the  $x$  direction as  $V_s = |V_{ix} - U_x| = 20$  km/s, which determines the Alfvén Mach number as  $M_A = V_s/V_A \approx 0.2$ . We perform a minimum variance analysis (MVA) [27] on these data with respect to  $B_x$ , which determines the direction of propagation of the structure along the  $x$  direction, from which we find the propagation angle  $\alpha \approx -83^\circ$ . The result of the MVA analysis is shown in Fig. 5(b).

In Fig. 7 we show the numerical solution of Eqs. (45) and (46) for the parameter regime of Fig. 5 and Table I. In

Fig. 7(a) we show the numerical solution, while in Fig. 7(b) we superimpose the numerical solution on the solution for our test case. Note that in the numerical calculation, the  $y$  axis is normalized to the ambient (average) magnetic field strength  $B_0 \sim 30$  nT while the  $x$  axis is normalized with the ion inertial length and the  $x = [0, 120]$  corresponds to the time range of  $\sim 220$  s from 08:59:02 to 09:03:00 (UT). As we can see that the numerical solutions can produce a similar train of solitons corresponding to the observed oscillations, which are largely in agreement. We note here that with different parameters, Eqs. (45) and (46) can also produce oscillations with decreasing amplitudes. It should be noted here that these numerical solutions are not expected to produce exactly what is observed experimentally because the oscillations picked up by the on-board instruments will also contain effects of microturbulence and magnetic reconnection [28]. However, what we see is that it can describe the overall behavior of these magnetosonic oscillations, which are mathematically within the realistic values of parameters.

To show the parameter space of the nonlinear domain, we perform a linear perturbation analysis of Eqs. (45) and (46). Assume a small perturbation of the dynamical quantities  $f \rightarrow f_0 + \delta f$ , where  $f_0$  and  $\delta f$  are, respectively, the equilibrium and perturbed parts and  $f = (b_y, b_z, n)$ . The resultant semilinearized perturbed equations are given by [12]

$$\begin{aligned} \frac{1}{M_x} \frac{\partial}{\partial x} \delta b_y &= \delta b_z \frac{1}{M_x^2} (1 - M_x^2) \left( 1 - \frac{1}{2} a_p \beta \right) + b_{z0} \delta n \\ &\quad - b_{z0} \frac{1}{2 M_x^2} a_p \beta \delta n^\gamma \delta b^{\kappa-2} - \beta_e \frac{1}{2 M_A} \frac{\partial}{\partial x} \delta n, \end{aligned} \quad (61)$$

$$\frac{1}{M_x} \frac{\partial}{\partial x} \delta b_z = -\frac{1}{M_x^2} \left( 1 - \frac{1}{2} a_p \beta \right) \delta b_y + \delta b_y, \quad (62)$$

where the last two terms of Eq. (61) are to be linearized. Considering the perturbation to be an oscillation in space of the form  $\delta f \sim e^{ikx}$  (where  $k$  is the linear wave number), the

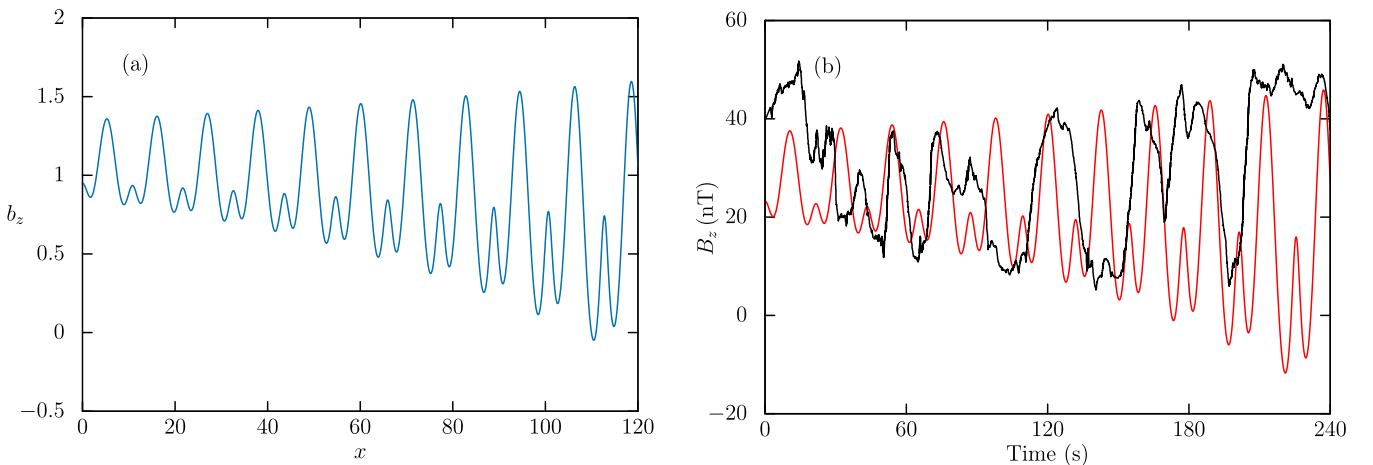


FIG. 7. A numerical solution of Eqs. (45) and (46) for the parameter regime shown in Fig. 5 and Table I.



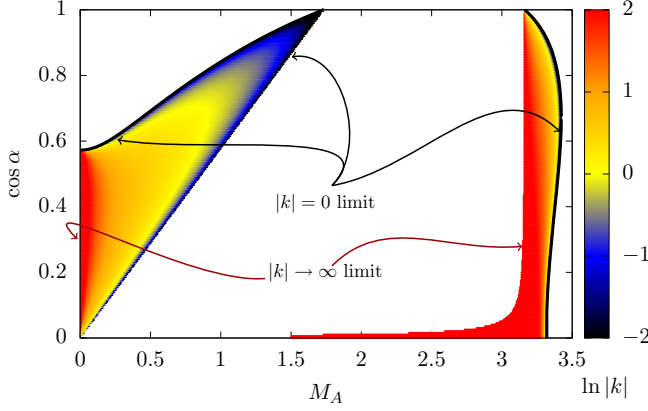


FIG. 8. Domain of nonlinear oscillations of Eqs. (45) and (46) in the  $M_A$ - $\cos \alpha$  plane for  $\beta = 20$ . The plasma parameters are taken from the *Cluster* observations (see Table I)  $a_p = -0.2$ ,  $\beta_e = 0.3$  with  $\gamma = 1$  and  $\kappa = 0$ . The value of  $|k|$  is color coded from black (small  $|k|$ ) to red (large  $|k|$ ).

resultant linear dispersion relation can be written as

$$\begin{aligned} & \frac{Ab_{z0}}{(\beta\gamma - 2M_A^2)} \left[ b_{z0} \left( 1 - \frac{\gamma a_p \beta}{2M_x^2} \right) - \frac{ik\beta_e}{2M_A} \right] \\ & + \frac{1}{2M_x^2} a_p \beta (1 + \kappa b_{z0}^2 - 2b_{z0}^2) - \frac{1}{M_x^2} \\ & - \frac{2k^2}{a_p \beta - 2(1 - M_x^2)} + 1 = 0, \end{aligned} \quad (63)$$

with

$$A = 2 + \beta\kappa + a_p \beta b_{x0}^2 (\kappa - 2). \quad (64)$$

The domain of linear oscillation of the system is now determined by the region of parameter space where solutions of  $k$  from Eq. (63) are real. Subsequently, the nonlinear domain is determined by purely imaginary solutions of  $k$ , which is shown in Fig. 8. As can be seen from Fig. 8, the oscillations shown in Fig. 5 and Table I are within the nonlinear domain.

## VI. SUMMARY AND CONCLUSIONS

In this paper, we have presented a nonlinear dynamical model based on the Hall-MHD equations with the FLR effect. The FLR term is incorporated into the analysis through the generalized Ohm's law. The ion pressure is modeled with the polybaric pressure equations, which is a generalized form of equation of state—a good and pliable approximation to the observed measurements [18]. The electron inertia is, however,

neglected in the generalized Ohm's law. The electron pressure is assumed to be isotropic. This modified Hall-MHD model can be reduced to two nonlinear coupled differential equations which describe the magnetosonic structures in its rest frame.

Through a bifurcation analysis of the resultant system, we have shown that this nonlinear model does not possess a limit cycle, which rules out regular periodic oscillations with constant amplitude. However, it does result in a train of magnetosonic solitons with amplitudes increasing in time, which are largely in agreement with what is usually observed in the magnetopause region. These oscillations can be called *aperiodic* in space. We emphasize that most of the train of solitary oscillations observed by the *Cluster* fleet and other spacecrafts do not have constant amplitudes: they either continuously increase or decrease. These trains of solitons with nonconstant amplitudes are a primary solution of our model. We also note that our model can reproduce train of solitons with either increasing or decreasing amplitudes in proper parameter space. It can be noted here that though these oscillations are thought to be a result of mirror-modes kinetic oscillations, it has been shown that similar oscillations can also result out of a Hall-MHD plasma model, which does not require a kinetic approach.

The numerical results obtained in this paper are for relevant parameter regimes reported by the *Cluster* spacecrafts and resultant oscillations show the same trend as the observed ones.

## ACKNOWLEDGMENTS

The authors gratefully acknowledge the *Cluster* CIS and FGM team for making the necessary data available for this research. M.K. is thankful to the Newton-Bhabha program for supporting the visit to the Rutherford Appleton Laboratory (RAL), UK. It is also a pleasure to thank Rajeev Pattathil, Gemini Group leader, CLF, STFC, RAL, and John Pasley, University of York, who have made this academic visit possible. The authors would also like to acknowledge Chris Perry of RAL and Anthony J. Allen, Space and Atmospheric Physics, Imperial College, London for their help in using the QSAS software. M.K. also acknowledges UGC, India, for awarding the UGC-BSR Fellowship during which this work has been carried out. The *Cluster* spacecraft data analysis was done with the QSAS science analysis system provided by the United Kingdom Cluster Science Centre (Imperial College London and Queen Mary, University of London) supported by the Science and Technology Facilities Council (STFC), UK. The authors would also like to thank the anonymous referees for a critical review.

- [1] S. Moola, R. Bharuthram, S. V. Singh, and G. S. Lakhina, *Pramana* **61**, 1209 (2003).
- [2] H. Matsumoto, H. Kojima, Y. Omura, M. Okada, I. Nagano, and M. Tsutsui, *Geophys. Res. Lett.* **21**, 2915 (1994).
- [3] J. De Keyser *et al.*, *Space Sci. Rev.* **118**, 231 (2005).
- [4] I. Silin, J. Büchner, and A. Vaivads, *Phys. Plasmas* **12**, 062902 (2005).

- [5] R. Trines, R. Bingham, L. O. Silva, J. T. Mendonça, P. K. Shukla, and W. B. Mori, *Phys. Rev. Lett.* **94**, 165002 (2005).
- [6] S. P. Joy, M. G. Kivelson, R. J. Walker, K. K. Khurana, C. T. Russell, and J. G. W. R. Paterson, *J. Geophys. Res.* **111**, A12212 (2006).
- [7] E. A. Lucek, D. Constantinescu, M. L. Goldstein, J. Pickett, J. L. Pincon, F. Sahraoui, R. A. Treumann, and S. N. Walker, *Space Sci. Rev.* **118**, 95 (2005).



- [8] R. Kaufmann, J. T. Horng, and A. Wolfe, *J. Geophys. Res.* **75**, 4666 (1970).
- [9] A. Hasegawa, *Phys. Fluids* **12**, 2642 (1969).
- [10] M. B. B. Cattaneo, C. Basile, G. Moreno, and J. D. Richardson, *J. Geophys. Res.* **103**, 11961 (1998).
- [11] B. T. Tsurutani, G. S. Lakhina, E. J. Smith, B. Buti, S. L. Moses, F. V. Coroniti, A. L. Brinca, J. A. Slavin, and R. D. Zwickl, *Nonlin. Proc. Geophys.* **6**, 229 (1999).
- [12] K. Stasiewicz, *Phys. Rev. Lett.* **93**, 125004 (2004).
- [13] K. Baumgärtel, K. Sauer, and E. Dubinin, *Geophys. Res. Lett.* **30**, 1761 (2003).
- [14] R. J. Goldston and P. H. Rutherford, *Introduction to Plasma Physics* (IOP, Bristol, UK, 1995).
- [15] D. M. Willis, *Geophys. J. Roy. Astron. Soc.* **41**, 355 (1975).
- [16] K. Stasiewicz, *Space Sci. Rev.* **65**, 221 (1994).
- [17] N. A. Krall and A. W. Trivelpiece, *Principles of Plasma Physics* (McGraw-Hill, New York, 1973).
- [18] K. Stasiewicz, *Phys. Rev. Lett.* **95**, 015004 (2005).
- [19] R. Kulsrud, in *Handbook of Plasma Physics: Basic Plasma Physics I*, edited by A. A. Galeev and R. N. Sudan (North-Holland, Amsterdam, 1983), Chap. 1.4, pp. 115–145.
- [20] S. H. Strogatz, *Nonlinear Dynamics and Chaos* (Perseus Books, Massachusetts, USA, 1994).
- [21] M. R. Ricard, *J. Phys. A* **44**, 065202 (2011).
- [22] I. Bendixson, *Acta Math.* **24**, 1 (1901).
- [23] H. Dulac, *C. R. Acad. Sci. Paris* **204**, 1703 (1937).
- [24] N. G. Lloyd, *J. London Math. Soc.* **s2-20**, 277 (1979).
- [25] J. Guckenheimer and P. Holmes, *Nonlinear Oscillations, Dynamical Systems, and Bifurcations of Vector Fields* (Springer-Verlag, New York and Tokyo, 1983).
- [26] P. M. E. Décréau *et al.*, *Space Sci. Rev.* **79**, 157 (1997).
- [27] B. U. Ö. Sonnerup and J. Cahill, *J. Geophys. Res.* **72**, 171 (1967).
- [28] M. Yamada, R. Kulsrud, and H. Ji, *Rev. Mod. Phys.* **82**, 603 (2010).